Strong-field macroscopic magneto-transport in a periodic composite medium: Some new results

2011 J. Phys.: Conf. Ser. 319 012002

(http://iopscience.iop.org/1742-6596/319/1/012002)

Journal of Physics: Conference Series **319** (2011) 012002 doi:10.1088/1742-6596/319/1/012002

Strong-field macroscopic magneto-transport in a periodic composite medium: Some new results

Yakov M. Strelniker[1] and David J. Bergman[2]

[1]Department of Physics, Bar-Ilan University, IL-52900 Ramat-Gan, Israel
[2]Raymond and Beverly Sackler School of Physics and Astronomy, Faculty of Exact Sciences, Tel Aviv University, IL-69978 Tel Aviv, Israel

E-mail: [1]strelnik@biu.ac.il, [2]bergman@post.tau.ac.il

Abstract. Results are reported of calculations of the macroscopic magnetoresistance of a two-constituent composite electrical conductor where the constituent resistivity tensors are comparable but different, and where the Hall resistivities are much greater than the Ohmic resistivities. Some of the macroscopic Ohmic resistivities fluctuate very strongly with the direction of the externally applied magnetic field $\mathbf{B}$ and keep increasing as $\mathbf{B}^2$ without any saturation.

1. Introduction

That the macroscopic response of a composite conductor with a periodic microstructure can be strongly anisotropic in the presence of a strong magnetic field was first realized in Refs. [1, 2]. In those references a simple-cubic array of insulating inclusions in an otherwise uniform and isotropic conducting host was studied numerically in the case where the Hall resistivity of the host was greater than its Ohmic resistivity. Some time after that some of those results were verified in experiments on a thin semiconducting film with an array of nano-holes [3] and on a bismuth film with a similar array of holes [4].

More recently it was realized that, even if all the constituents are electrical conductors with comparable though different resistivity tensors, the magneto-transport can exhibit dramatic new forms of behavior. These include new critical points in the case of a disordered microstructure [5, 6, 7, 8] and strongly anisotropic magnetoresistance when the Hall-to-Ohmic resistivity ratio is much greater than 1 in all the constituents [9].

This article reports on some new results regarding the macroscopic magneto-transport of a two-constituent composite medium with a periodic microstructure in the regime where the externally applied magnetic field $\mathbf{B}$ is strong enough that the Hall resistivity is much greater than the Ohmic resistivities in both constituents. Both of those constituents are electrical conductors with different but comparable resistivity tensors. Therefore this article reports on an extension of calculations that were described in more detail in Ref. [9].

Among the noteworthy results is the fact that the macroscopic transverse Ohmic resistivities show tremendous fluctuations with changes in the direction of the magnetic field $\mathbf{B}$, and that for some directions the magnitude of those resistivities appears to increase as $\mathbf{B}^2$.

In Section 2 we briefly describe the numerical approach used to compute the macroscopic magnetoresistivity tensor $\hat{\rho}_e$ of a two-constituent periodic composite. In Section 3 we describe

some results of those computations. In Section 4 we discuss those results and summarize some of their implications, including some potential applications.

2. Numerical computations for a periodic composite medium

We use a scheme that is described in detail in Ref. [2]. For completeness, we present here a brief description of that scheme, which was also used to calculate all the numerical results reported in Ref. [9].

Ordinarily, the local electric potential $\phi^{(\alpha)}(\mathbf{r})$, produced in the system when the volume-averaged electric field is $\langle \mathbf{E} \rangle = \mathbf{e}_\alpha$, would be found by solving the following standard boundary value problem

$$\begin{aligned} &\nabla \cdot [\hat{\sigma}(\mathbf{r}) \cdot \nabla \phi^{(\alpha)}(\mathbf{r})] = 0 \ \text{ in the entire volume } V, \\ &\phi^{(\alpha)}(\mathbf{r}) = r_\alpha \qquad \text{at the external surface } \partial V, \end{aligned}$$

where

$$\begin{aligned} \hat{\sigma}(\mathbf{r}) &= \hat{\sigma}_1 \theta_1(\mathbf{r}) + \hat{\sigma}_2 \theta_2(\mathbf{r}) \equiv \hat{\sigma}_2 - \theta_1(\mathbf{r}) \delta\hat{\sigma}, \\ \delta\hat{\sigma} &\equiv \hat{\sigma}_2 - \hat{\sigma}_1, \\ \theta_i(\mathbf{r}) &= 1 \ \text{ if } \ \hat{\sigma}(\mathbf{r}) = \hat{\sigma}_i \ \text{ and } \ \theta_i(\mathbf{r}) = 0 \ \text{ otherwise.} \end{aligned}$$

Instead of doing that, we first use a Green's function of this problem in a uniform conductor $\hat{\sigma}_2$, denoted by $G(\mathbf{r}, \mathbf{r}' | \hat{\sigma}_2)$, to transform this partial differential equation with boundary conditions to an integrodifferential equation:

$$\phi^{(\alpha)} = r_\alpha + \hat{\Gamma} \phi^{(\alpha)}, \tag{1}$$

$$\hat{\Gamma}\phi \equiv \int dV' \theta_1(\mathbf{r}') \nabla' G(\mathbf{r}, \mathbf{r}' | \hat{\sigma}_2) \cdot \delta\hat{\sigma} \cdot \nabla' \phi^{(\alpha)}(\mathbf{r}'), \tag{2}$$

$$\begin{aligned} G(\mathbf{r}, \mathbf{r}' | \hat{\sigma}) &\equiv \int \frac{d^3k}{(2\pi)^3} \frac{e^{i\mathbf{k}\cdot(\mathbf{r}-\mathbf{r}')}}{(\mathbf{k} \cdot \hat{\sigma} \cdot \mathbf{k})} = \frac{1}{4\pi(\sigma_{xx}\sigma_{yy}\sigma_{zz})^{1/2}} \\ &\times \left(\frac{(x-x')^2}{\sigma_{xx}} + \frac{(y-y')^2}{\sigma_{yy}} + \frac{(z-z')^2}{\sigma_{zz}} \right)^{-1/2}. \end{aligned} \tag{3}$$

If the microstructure is spatially periodic, then $\psi^{(\alpha)}(\mathbf{r}) \equiv \phi^{(\alpha)}(\mathbf{r}) - r_\alpha$ is a similarly periodic function of $\mathbf{r}$ and we expand it in an appropriate Fourier series,

$$\psi^{(\alpha)}(\mathbf{r}) = \sum_{\mathbf{g} \neq 0} \psi_{\mathbf{g}}^{(\alpha)} e^{i\mathbf{g}\cdot\mathbf{r}}, \tag{4}$$

where the sum is over all the nonzero vectors $\mathbf{g}$ of the appropriate reciprocal lattice. Equation (1) is thereby transformed into an infinite set of linear algebraic equations for the coefficients $a_{\mathbf{g}}^{(\alpha)} \equiv i(\mathbf{g} \cdot \hat{\sigma}_2 \cdot \mathbf{g})^{1/2} \psi_{\mathbf{g}}^{(\alpha)}$, where $\mathbf{g} \neq 0$,

$$a_{\mathbf{g}}^{(\alpha)} = r_{\mathbf{g}}^{(\alpha)} + \sum_{\mathbf{g}' \neq 0} \Gamma_{\mathbf{g}\mathbf{g}'} a_{\mathbf{g}'}^{(\alpha)} \quad \text{for} \quad \mathbf{g} \neq 0, \tag{5}$$

$$r_{\mathbf{g}}^{(\alpha)} \equiv \frac{g_\beta \delta\sigma_{\beta\alpha}}{(\mathbf{g} \cdot \hat{\sigma}_2 \cdot \mathbf{g})^{1/2}} \theta_{\mathbf{g}}, \tag{6}$$

$$\theta_{\mathbf{g}} = \frac{1}{V_a} \int_{V_a} d^3r \theta_1(\mathbf{r}) e^{i\mathbf{g}\cdot\mathbf{r}}, \tag{7}$$

$$\Gamma_{\mathbf{g}\mathbf{g}'} \equiv \frac{(\mathbf{g} \cdot \delta\hat{\sigma} \cdot \mathbf{g}')}{(\mathbf{g} \cdot \hat{\sigma}_2 \cdot \mathbf{g})^{1/2} (\mathbf{g}' \cdot \hat{\sigma}_2 \cdot \mathbf{g}')^{1/2}} \theta_{\mathbf{g}-\mathbf{g}'}, \tag{8}$$

where V_a is the volume of one unit cell. After a truncated subset of Eqs. (5) are solved for $a_{\mathbf{g}}^{(\alpha)}$, the fields $\phi^{(\alpha)}$, $\mathbf{E}^{(\alpha)}$ and the elements of the macroscopic conductivity tensor $\hat{\sigma}_e$ can be calculated as follows:

$$\phi^{(\alpha)} = r_\alpha + \psi^{(\alpha)} = r_\alpha + \sum_{\mathbf{g}\neq 0} \frac{a_{\mathbf{g}}^{(\alpha)}}{i(\mathbf{g}\cdot\hat{\sigma}_2\cdot\mathbf{g})^{1/2}} e^{i\mathbf{g}\cdot\mathbf{r}}, \tag{9}$$

$$E_\beta^{(\alpha)} = \nabla_\beta \phi^{(\alpha)} = \delta_{\alpha\beta} + \sum_{\mathbf{g}\neq 0} \frac{g_\beta a_{\mathbf{g}}^{(\alpha)}}{(\mathbf{g}\cdot\hat{\sigma}_2\cdot\mathbf{g})^{1/2}} e^{i\mathbf{g}\cdot\mathbf{r}}, \tag{10}$$

$$\sigma_{\alpha\beta}^{(e)} = \langle\sigma_{\alpha\beta}\rangle - \sum_{\mathbf{g}\neq 0} \frac{\delta\sigma_{\alpha\beta} g_\beta}{(\mathbf{g}\cdot\hat{\sigma}_2\cdot\mathbf{g})^{1/2}} \theta_{-\mathbf{g}} a_{\mathbf{g}}^{(\beta)}. \tag{11}$$

Note that the coefficient multiplying $a_{\mathbf{g}}^{(\beta)}$ in the last sum looks similar to $r_{\mathbf{g}}^{(\alpha)*}$, but actually differs from it, because $\delta\sigma_{\alpha\beta} \neq \delta\sigma_{\beta\alpha}$.

Because the characteristic function $\theta_1(\mathbf{r})$ is discontinuous at the $\hat{\sigma}_1$-$\hat{\sigma}_2$ interface, the local electric field also is discontinuous there. Consequently the Fourier coefficients of both functions decrease very slowly for large $\mathbf{g}$. For this reason a very large number of the coefficients $a_{\mathbf{g}}^{(\alpha)}$ need to be used in Eqs. (9)–(11) in order to get accurate results. This means that a large number of the coupled linear algebraic Eqs. (5) must be kept and solved, which requires huge computing time and memory resources.

An alternative procedure, which is less demanding in terms of those resources, is to solve those equations by iterative application of the $\Gamma_{\mathbf{g}\mathbf{g}'}$ matrix, i.e., by computing the nth term $a_{\mathbf{g}n}^{(\alpha)}$ in the infinite series

$$a_{\mathbf{g}}^{(\alpha)} = \sum_{n=0}^{\infty} a_{\mathbf{g}n}^{(\alpha)} \tag{12}$$

iteratively by

$$a_{\mathbf{g}0}^{(\alpha)} = r_{\mathbf{g}}^{(\alpha)}, \quad a_{\mathbf{g}n}^{(\alpha)} = \sum_{\mathbf{g}'\neq 0} \Gamma_{\mathbf{g}\mathbf{g}'} a_{\mathbf{g}'n-1}^{(\alpha)}. \tag{13}$$

The expression [Eq. (12)] obtained by this procedure is a series in powers of the $\Gamma_{\mathbf{g}\mathbf{g}'}$ matrix elements. Those elements are sometimes very large, consequently the series is often strongly divergent. In those cases advanced methods must be employed in order to get useful results from that series. Because of this, the computations reported in this paper are all based upon numerical solution of a truncated subset of Eqs. (5), in which more than 9000 of the $a_{\mathbf{g}}^{(\alpha)}$ coefficients were calculated. That is, the components of $\mathbf{g}$ in each direction went up to $\pm 2\pi n/a$, where a is the unit cell edge and the integer n was between 10 and 15. Because this limited number of Fourier components is not sufficient to represent the discontinuous functions $\theta_1(\mathbf{r})$ and $\mathbf{E}(\mathbf{r})$ accurately, therefore the detailed numerical results for $\mathbf{E}(\mathbf{r})$, obtained by using Eq. (10), often exhibit spurious spatial oscillations—see Ref. [9]. Nevertheless, when the computed Fourier coefficients are used to calculate the macroscopic conductivity tensor $\hat{\sigma}^{(e)}$, using Eq. (11), the results are quite accurate. This was demonstrated in Ref. [9] by comparing the numerically computed results for $\hat{\sigma}^{(e)}$ with the results of an exact asymptotic theory for large values of the Hall-to-Ohmic resistivity ratio.

3. Results of computations for the macroscopic magnetoresistivity tensor $\hat{\rho}_e \equiv 1/\hat{\sigma}_e$

We consider a simple-cubic array of spherical inclusions with radius R given by $R/a = 0.4$, where $a \times a \times a$ is the unit cell size, and characterized by the resistivity tensor $\hat{\rho}_1$. These inclusions

are embedded in an otherwise uniform host characterized by the resistivity tensor $\hat{\rho}_2$. Both constituents are assumed to be isotropic media, thus their resistivity tensors can be written in the form

$$\hat{\rho}_i = \rho_0 \begin{pmatrix} \alpha_i & -\beta_i & 0 \\ \beta_i & \alpha_i & 0 \\ 0 & 0 & \lambda_i \end{pmatrix}, \quad i = 1, 2. \tag{14}$$

These two tensors are different but comparable, and their form assumes that the z-axis lies along the external magnetic field $\mathbf{B}$. Clearly, $\rho_0\alpha_i$ are the transverse Ohmic resistivities, $\rho_0\lambda_i$ are the longitudinal Ohmic resistivities, $\rho_0\beta_i = R_{Hi}|\mathbf{B}|$ are the Hall resistivities, where R_{Hi} are the Hall coefficients. We assume that ρ_0 characterizes the common magnitude of the four relevant Ohmic resistivities, i.e., α_1, α_2, λ_1, λ_2 are all dimensionless parameters of order $\mathcal{O}(1)$. We also assume that the externally applied uniform magnetic field is strong enough so that both β_1 and β_2 are much greater than 1, i.e., that the Hall-to-Ohmic resistivity ratio β_i/α_i is much greater than 1. From Eq. (14) we immediately get the following form for the conductivity tensors of the two constituents:

$$\hat{\sigma}_i \equiv \frac{1}{\hat{\rho}_i} = \frac{1}{\rho_0} \begin{pmatrix} \frac{\alpha_i}{\alpha_i^2+\beta_i^2} & \frac{\beta_i}{\alpha_i^2+\beta_i^2} & 0 \\ \frac{-\beta_i}{\alpha_i^2+\beta_i^2} & \frac{\alpha_i}{\alpha_i^2+\beta_i^2} & 0 \\ 0 & 0 & \frac{1}{\lambda_i} \end{pmatrix}. \tag{15}$$

This is used to compute the elements of the macroscopic conductivity tensor $\hat{\sigma}_e$, and subsequently those of the macroscopic resistivity tensor $\hat{\rho}_e \equiv 1/\hat{\sigma}_e$.

In Fig. 2 we show results for the diagonal elements of $\hat{\rho}_e$ for the case where the y axis is fixed along the (010) lattice axis of the cubic array, while the magnetic field $\mathbf{B}$ is continuously rotated in the perpendicular plane, along with the axes x' and z', by the angle θ—see Fig. 1(a). Results are shown for two different values of the β_i, while keeping fixed the ratio β_1/β_2 and also all of the other constituent parameters. In lines 1 and 3 the elements of $\hat{\rho}_e$ are taken with respect to the fixed coordinate system, namely $x \parallel (100)$, $y \parallel (010)$, $z \parallel (001)$, even though the direction of $\mathbf{B} \parallel z'$ keeps changing with changing θ, since θ is the angle between the rotating z' axis and the fixed $z \parallel (001)$ axis. In lines 2 and 4 the elements of $\hat{\rho}_e$ are taken with respect to the rotating coordinate system, where the z' and x' axes are inclined by θ with respect to the fixed $z \parallel (001)$ and $x \parallel (100)$ axes respectively.

In Fig. 3 we show similar plots for another kind of rotation of the direction of $\mathbf{B}$: The y' axis is fixed along the (011) lattice axis, while the other two fixed axes are $x \parallel (100)$, $z' \parallel (0\bar{1}1)$. The magnetic field $\mathbf{B}$ is then rotated in the plane perpendicular to the y' axis, which remains fixed along the (011) lattice axis, and θ is the angle between $\mathbf{B}$ and the fixed $z' \parallel (0\bar{1}1)$ axis—see Fig. 1(b),(c). In lines 1 and 3 the elements of $\hat{\rho}_e$ are taken with respect to the fixed lattice coordinates $x \parallel (100)$, $y \parallel (010)$, $z \parallel (001)$ and plotted vs. θ. In lines 2 and 4 the elements of $\hat{\rho}_e$ are taken with respect to the rotating coordinates x'', y', z'', i.e., although $y' \parallel (011)$ is fixed, the x'' and z'' axes rotate around y' so that z'' remains oriented along the rotating $\mathbf{B}$. The results in all parts of Fig. 3 are plotted vs. the angle θ between $\mathbf{B} \parallel z''$ and the fixed $z' \parallel (0\bar{1}1)$ axis.

4. Discussion of the results

When $y \parallel (010)$ is kept fixed, $\rho_{yy}^{(e)}$ exhibits strong oscillations—see Fig. 2(b),(e),(h),(m). Comparing Fig. 2(b),(e), (which are identical) and Fig. 2(h),(m) (which are also identical) shows that, for most values of θ, $\rho_{yy}^{(e)}$ appears to increase as β_i^2 when the ratio β_1/β_2, as well as all the other constituent parameters, are kept fixed. Because the Hall resistivities of electrical conductors are usually simply proportional to the magnitude of the magnetic field $\mathbf{B}$, therefore this means that usually $\rho_{yy}^{(e)} \propto |\mathbf{B}|^2$. Deviations from this behavior occur when $\mathbf{B}$ lies along a high symmetry lattice axis, e.g., a (001)-like axis or a (011)-like axis. At those orientations $\rho_{yy}^{(e)}$

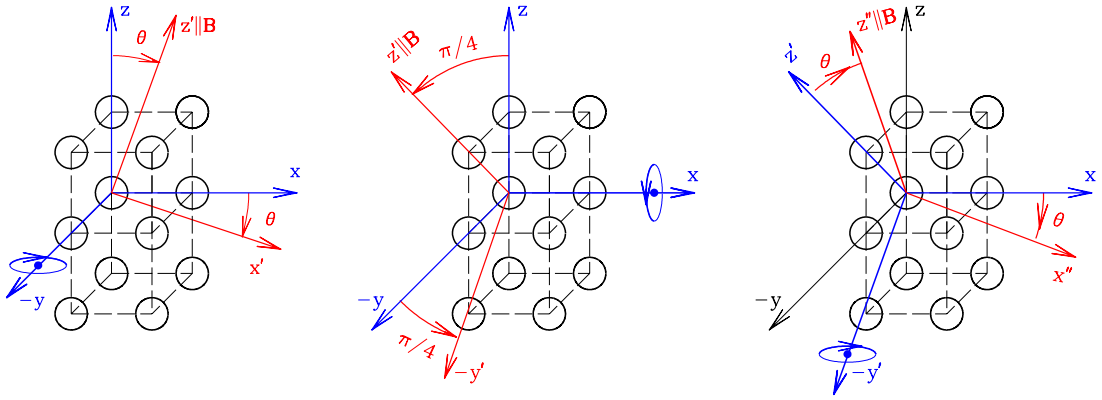

Figure 1. (Color online) The geometry described in (a) is used to get the results shown in Fig. 2, while the geometry described in (b) and (c) is used to get the results shown in Fig. 3. (a) The axis $y \parallel (010)$ is kept fixed while the axes x' and z' subtend a changing angle θ with the fixed $x \parallel (100)$ and $z \parallel (001)$ axes, respectively, and remain perpendicular to y. (b) New fixed axes $y' \parallel (011)$, $z' \parallel (0\bar{1}1)$ are obtained by a $\pi/4$ rotation about the x axis. (c) The $y' \parallel (011)$ axis is kept fixed while the axes x'' and z'' subtend a changing angle θ with the fixed axes $x \parallel (100)$ and $z' \parallel (0\bar{1}1)$, respectively, and remain perpendicular to y'.

also exhibits a sharp minimum as function of θ. By contrast, the longitudinal component $\rho_{zz}^{(e)}$ in Fig. 2(f),(n), i.e., the Ohmic component of $\hat{\rho}_e$ along $\mathbf{B}$, is nearly independent of θ and of the two β_i if the ratio β_1/β_2 is kept fixed. The other transverse Ohmic resistivity component $\rho_{xx}^{(e)}$—see Fig. 2(d),(l)— does oscillate as function of θ and changes with the β_i, but does not increase significantly when the β_i are increased by a factor of 10.

Turning to the other kind of rotations, shown in Fig. 1(b),(c), we note that now $y' \parallel (011)$ and $z' \parallel (0\bar{1}1)$ are kept fixed. In this case too $\rho_{yy}^{(e)}$ exhibits oscillations—see Fig. 3(b),(e),(h),(m). It also increases with the β_i, but not as rapidly as β_i^2. Again, the longitudinal Ohmic component $\rho_{zz}^{(e)}$ in Fig. 3(f),(n) is constant as function of θ and of the two β_i if the ratio β_1/β_2 is kept fixed. The most interesting behavior is exhibited by the other transverse Ohmic resistivity component $\rho_{xx}^{(e)}$ in Fig. 3(d),(l): For most values of θ it is quite small and does not increase significantly when the β_i are increased by a factor of 10. However, when $\mathbf{B}$ lies along some special directions $\rho_{xx}^{(e)}$ exhibits a sharp maximum where its value is very large and appears to increase as β_i^2—see the cases $\theta = 0$ and $\theta = \pi/2$, i.e., $\mathbf{B}$ lies along $(0\bar{1}1)$ and along (001), respectively, and the cases $\theta = \pi/4$ and $\theta = 3\pi/4$. In the last two cases the direction of $\mathbf{B}$ does not correspond to any simple or high symmetry lattice axis. As we mentioned before, this behavior means that, at those peaks, we usually will expect to find $\rho_{xx}^{(e)} \propto |\mathbf{B}|^2$.

The strongly oscillating behavior described in the preceding two paragraphs is not yet well understood. It may possibly be exploitable in making a magnetic field sensor for a strong magnetic field $\mathbf{B}$ that is sensitive to the magnitude as well as to the direction of $\mathbf{B}$. This is particularly true of the behavior exhibited by $\rho_{xx}^{(e)}$ in Fig. 3(d),(l), where the peaks at $\theta = 0$ and $\theta = \pi/2$ are extremely high, narrow, and isolated, and their height appears to increase as $|\mathbf{B}|^2$.

The results and predictions reported here all arise from numerical computations of the local electric field and current distributions in a periodic composite conductor in the presence of a strong magnetic field. Those results and predictions need to be tested in experiments. We hope this challenge will be taken up by experimentalists who have the necessary equipment and

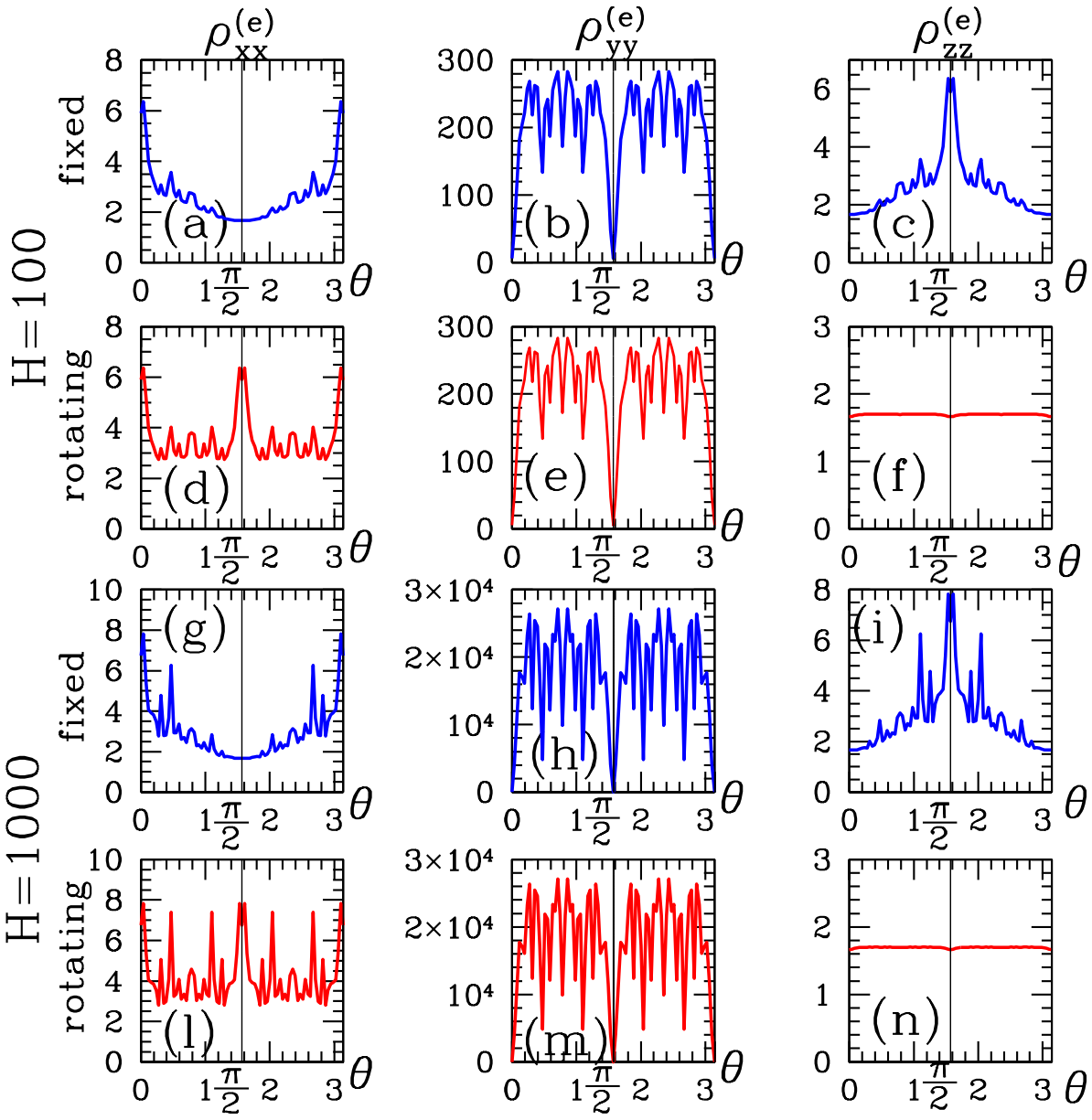

Figure 2. (Color online) All the results are for a simple-cubic array of spherical inclusions with radii R given by $R = 0.4a$, where a is the edge length of a unit cell. The inclusions are characterized by the resistivity tensor $\hat{\rho}_1$ and are embedded in an otherwise uniform host characterized by the resistivity tensor $\hat{\rho}_2$. Lines 1 and 2 show results when $\rho_0 = 1$, $\alpha_1 = 1$, $\alpha_2 = 2$, $\lambda_1 = 1$, $\lambda_2 = 2$, $\beta_1 = 100$, $\beta_2 = 200$. Lines 3 and 4 show results for the same physical parameters with the exception of $\beta_1 = 1000$, $\beta_2 = 2000$, i.e., both Hall resistivities are larger by a factor 10. (a)–(c) $\rho^{(e)}_{xx}$, $\rho^{(e)}_{yy}$, and $\rho^{(e)}_{zz}$ plotted vs. the rotation angle θ of Fig. 1(a) but where these components are taken along the *fixed coordinates* x, y, z of Fig. 1(a),(b). (d)–(f) Similar to panels (a)–(c), but now the components of $\hat{\rho}_e$ are taken along the *rotating coordinates* x, y', z' of Fig. 1(b). (g)–(n) The same as panels (a)–(f) but with values of the two β_i's that are larger by a factor 10. It is useful to note that panels (e), (f), (d) correspond to α_e, λ_e, $\tilde{\alpha}_e$ which are shown as polar plots in the top line of panels in Fig. 13 of Ref. [9]. Similarly, panels (m), (n), (l) correspond in a similar fashion to α_e, λ_e, $\tilde{\alpha}_e$ which are shown in the top line of panels in Fig. 14 of that reference.

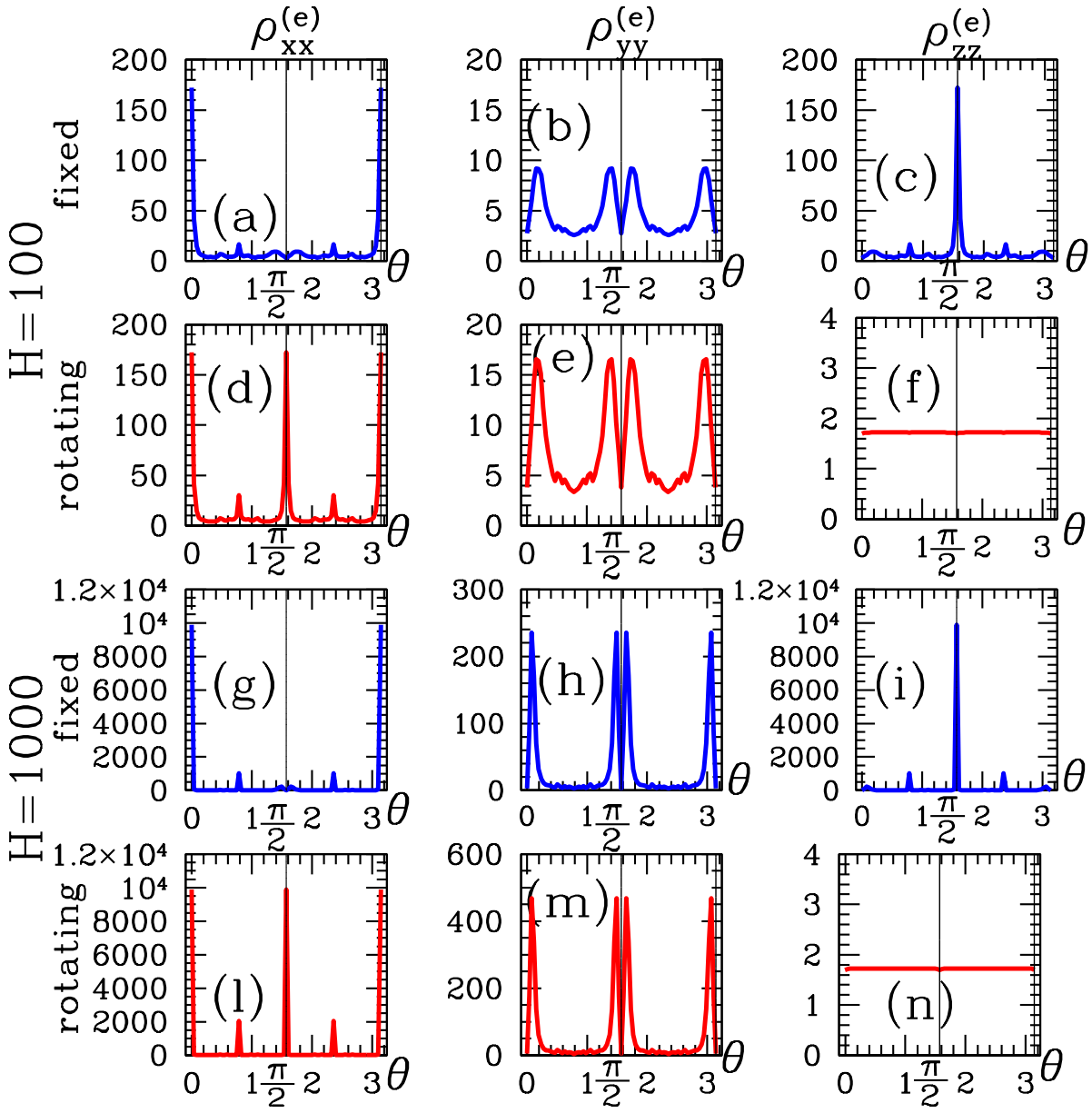

Figure 3. (Color online) Similar to Fig. 2 but now the fixed coordinate systems are $x \parallel (001)$, $y \parallel (010)$, $z \parallel (001)$ and $x \parallel (001)$, $y' \parallel (011)$, $z' \parallel (0\bar{1}1)$, while x'' and z'' subtend a changing angle θ with x and z', respectively, and remain perpendicular to y'—see Fig. 1(b) and (c). Note that the θ axis in all the panels stretches from -0.1 up to $\pi + 0.1$ in order to clarify the violent behavior of some of the plots near $\theta = 0$ and $\theta = \pi$. We note that the orientations of **B** reached in these plots were not considered in any previous reference, including Ref. [9].

expertise.

Acknowledgments
Partial support for this research was provided by grants from the U.S.-Israel Binational Science Foundation and the Israel Science Foundation and the Russia-Israel research program of the Science Ministry of the State of Israel, and by KAMEA Program (for YMS) of the Ministry of Absorption of the State of Israel.

References

[1] Bergman D J and Strelniker Y M 1994 *Phys. Rev. B* **49** 16256
[2] Strelniker Y M and Bergman D J 1994 *Phys. Rev. B* **50** 14001
[3] Tornow M, Weiss, D Klitzing K. v., Eberl K, Bergman D J, and Strelniker Y M 1996 *Phys. Rev. Lett.* **77** 147
[4] Strijkers G J, Yang F Y, Reich D H, Chien C L, Searson P C, Strelniker Y M, and Bergman D J 2001 *IEEE Trans. Magn.* **37** 2067
[5] Guttal V and Stroud D 2005 *Phys. Rev. B* **71** 201304
[6] Guttal V and Stroud D 2006 *Phys. Rev. B* **73** 085202
[7] Magier R and Bergman D J 2006 *Phys. Rev. B* **74**, 094423
[8] Magier R and Bergman D J 2008 *Phys. Rev. B* **77** 144406
[9] Bergman D J and Strelniker Y M 2010 *Phys. Rev. B* **82** 174422